Asian Journal of Chemistry; Vol. 34, No. 3 (2022), 597-606

ASIAN JOURNAL OF CHEMISTRY

https://doi.org/10.14233/ajchem.2022.23560

Study of Anticorrosive Action and Synthesis of 2-(Phenoxymethyl)-5-*p*-tolyl-1,3,4-oxadiazole in 1 M Hydrochloric Acid Medium for Mild Steel

SURESH KUMAR, VIKAS KALIA and HARIOM DAHIYA*

Department of Chemistry, M.D. University, Rohtak-124001, India

*Corresponding author: E-mail: hariom.chem@mdurohtak.ac.in

Received: 1 October 2021; *Accepted*: 24 November 2021; *Published online*: 14 February 2022; AJC-20691

Oxadiazole derivative 2-(phenoxymethyl)-5-*p*-tolyl-1,3,4-oxadiazole (2POM5PTO) was prepared by condensation of phenoxymethyl hydrazine with *p*-tolualdehyde. Further tested as corrosion inhibitor for mild steel *via* electrochemical methods, potentiodynamic polarization (PDP) and gravimetric experiments. An increasing trend in inhibition efficiency has been seen on raising the concentration of 2POM5PTO. PDP technique reveals the mixed-type inhibitor behaviour of 2POM5PTO. The depressed semicircular Nyquist plot explains that the charge transfer resistance increased with inhibitor concentration while double-layer capacitance (C_{dl}) decreased. The surface elucidation was done by scanning electron microscopy. The studied inhibitor obeys the Langmuir adsorption isotherm.

Keywords: Oxadiazole derivative, Electrochemical methods, Corrosion control, Mild steel, percentage inhibition efficiency.

INTRODUCTION

Mild steel is vital in developing infrastructure for the oil pipes, automobile sector, petrochemical industries, oil pipes and storage tanks. However, it has the drawback of weak susceptibility against corrosion in competitive conditions and demands safety to make sure a possible lifespan [1]. The inorganic acids (HCl, H_2SO_4, HNO_3) are broadly utilized in numerous industrial processes, including cleaning, descalling, pickling, oil well cleaning, *etc*. Acids show aggressiveness when they come in contact with metal. They deteriorate the metal *via* corrosion. So many researchers have been working in finding reasonable solutions which reduce mild steel corrosion and provide suitable protection [2]. The organic compounds, which retard the corrosion rate are called corrosion inhibitors. Organic compounds have π-electron and lone pair containing elements like P, N, O and S in their structure are efficient inhibitors. They protect the mild steel from deterioration in aggressive media by grabbing the mild steel. Also, the high electron density of organic compounds protects metals from corrosion *via* donating an electron or forming a coordination bond with an empty *d*-orbital of metal. For example, 2,5-disubstituted oxadiazole has anticancer, antitumor and anticorrosive behaviour [3-7]. These compounds were studied as corrosion inhibitors for mild steel in aggressive media [8].

In present work, a new compound 2,5-disubstituted oxadiazole, namely 2-(phenoxymethyl)-5-*p*-tolyl-1,3,4-oxadiazole (2POM5PTO) was synthesized and tested as corrosion inhibitor on mild steel in 1 M HCl solution at 298-318 K for 12 h. To evaluate the efficiency of 2POM5PTO as a corrosion inhibitor, weight loss measurement, electrochemical impedance spectroscopy and potentiodynamic polarization techniques were applied. Furthermore, the adsorption, thermodynamic parameters were calculated and discussed. Meanwhile, scanning electron microscopy (SEM) and energy-dispersive X-ray spectroscopy (EDAX) techniques were employed to analyze the surface of mild steel specimens [8]. In addition, density function theory was used to investigate the electronic property of 2-(phenoxymethyl)-5-*p*-tolyl-1,3,4-oxadiazole.

EXPERIMENTAL

Synthesis of 2-(phenoxymethyl)-5-*p*-tolyl-1,3,4-oxadiazole: Phenoxyhdrazide was mixed with *p*-tolualdehyde in a round bottom flask and stirred with heating mantle followed by the addition of sodium acetate (0.5 mmol) dropwise after 10 min. The solvent of the reaction mixture was evaporated

This is an open access journal, and articles are distributed under the terms of the Attribution 4.0 International (CC BY 4.0) License. This license lets others distribute, remix, tweak, and build upon your work, even commercially, as long as they credit the author for the original creation. You must give appropriate credit, provide a link to the license, and indicate if changes were made.

under reduced pressure. Further, a mixture of K_2CO_3 (2.5 mmol) and I_2 (1.5 mmol) was poured into the resultant mixture using 10 mL of 1,4-dioxane as solvent. Then the whole obtained mixture was put on heating mantle for 6 h at 100 ºC (monitored by TLC, 2-3 h). The reaction mixture was cooled overnight and then dried with 10% $Na_2S_2O_3$ and produce with CH_2Cl_2/MeOH (20:2, 20 mL × 5). Na_2SO_4 was used as a drying agent for the organic layer and purification was done through silica gel column chromatography using a mixture of ethyl acetate and petroleum ether as mobile phase to afford the corresponding 2-(phenoxymethyl)-5-*p*-tolyl-1,3,4-oxadiazole yield 85-99% [9]. IR (KBr, ν_{max} cm^{-1}): 1305.06 (C = N), 2957.19, 2835.29 (CH_2), 3057.57, 1208.26, 1179.38 and 1208.26 (arom. *str.* C-O-C), 2853.74 (arom. CH_3). ^{1}H NMR (DMSO-d_6): δ 6.944-8.30 (m) 9H, 5.122 (S) 2H, 2.33 (S) 3H.

Specimen and corrosive medium preparation: Mild steel (MS) samples having chemical composition (wt%): Cr = 0.056, Cu = 0.010, Si = 0.015, Ti = 0.002, S = 0.017, P = 0.019, Mo = 0.018, C = 0.054, Ni = 0.009 Mn = 0.26, rest Fe were used for various experiments. All the MS coupons were cut into 3 cm × 1.5 cm size and then employed to weight loss measurement. Prior to start tests, all samples were cleaned by hand rubbing (100, 200, 400, 600, 1000 and 1500 grade of emery papers) to provide them smooth surface, then cleaned by deionized water, diluted with acetone, dried with air blower, preserved into desiccators for further experimental studies. A HCl (1 M) aggressive solution was prepared using dilution (AR grade 37% of HCl) method. Same used in preparing of inhibitor solution of an optimum concentration. All the experiments were performed in 1 M HCl and adding different concentrations of 2-(phenoxymethyl)-5-*p*-tolyl-1,3,4-oxadiazole (2POM5PTO).

Weight loss technique: The rectangular mild steel (MS) coupons of dimension 3 cm × 1.5 cm × 0.1 cm were immersed in 1 M HCl medium containing optimum concentration of 2POM5PTO and 1 M HCl only for duration of 12 h at 298-318 K. The percentage inhibition efficiency was calculated by the following formula [10]:

$$\eta_w\ (\%) = \frac{w_o - w_i}{w_o} \times 100 \quad (1)$$

$$\theta = \frac{w_o - w_i}{w_o} \quad (2)$$

where w_o and w_i are the weight loss of mild steel in 1 M HCl only and 1 M HCl having various concentrations of 2POM5PTO, respectively. The following equation was used to compute the corrosion rate:

$$C_R\,(mm\ y^{-1}) = \frac{87.6 \times W}{AtD} \quad (3)$$

where w (mg), A (cm^2), t (h), D (g cm^{-3}) is weight loss of mild steel, area of the sample, exposure time and the density of mild steel, respectively.

Electrochemical measurements: Both potentiodynamic polarization and electrochemical spectroscopy tests were carried out using Ametek potentiostat/galvanostat (prastat-4000). The instrument assembled three electrodes (saturated calomel reference electrode, Pt auxiliary electrode counter electrode and (1 cm^2 area) mild steel sample). The potential range of ± 250 mV was used to perform the electrochemical test with a scan rate of 0.5 V/s. Tafel extrapolation provides different parameters, like corrosion current density, cathodic (β_c) and anodic (β_a) Tafel constant. The EIS experiments were conducted at open circuit potential (OCP) using ± 10 mV perturbation in a frequency range from 10 kHz to 10 MHz. Prior to star test, samples were left immersed in the solution for 30 min. The Z-view software was used to analyze the impedance data and all the experiments were repeated three times [11].

Surface analysis: Mild steel samples were prepared for surface analysis by putting them in a solution of 2POM5PTO in 1 M HCl and in pure 1 M HCl solution for 72 h. Before analysis, samples were washed with deionized water and acetone, dried with a hot air blower. For morphological study SEM-EDAX instrument (JEOL-JSM6510) was used [8].

DFT studies: Density functional theory (DFT) was used to analyze the electronic property of 2POM5PTO. The Dmol^3 module was used for all quantum calculations. The molecular modelling studies were carried out by using Gaussian 09 and Gauss View 5.0 program using B3LYP hybrid functional (Becke's three-parameter Lee-Yang-Par correlation functional) with all the electron Pople triple-ζ basis set along with two polarization functions 6-311G** [8] on the heavier atoms. All DFT parameters have been estimated in the aqueous phase using COSMO controls [12]. The hardness, electron affinity, electro negativity and ionization potential were calculated following Koopmans's theorem by applying equations:

$$IP = -E_{HOMO} \quad (4)$$

$$EA = -E_{LUMO} \quad (5)$$

$$\chi = \frac{IP + EA}{2} \quad (6)$$

$$\eta = \frac{IP - EA}{2} \quad (7)$$

Molecular dynamics (MD) simulation: The MD simulations were performed to investigate the adsorption of 2POM5PTO. Material Studio data base used for the Fe (110) plane selection. A large surface for the interaction of the inhibitor with the iron surface is provided through expanding the Fe (110) surface. The simulation box has two layers created in material Studio through layer built method to make the simulation as closer to the existing system as possible [12]. The first layer contained iron atoms, the layer above had $9H^+$, 500 H_2O, $9Cl^-$ and a monomer layer of inhibitor. All simulations were executed by COMPASSII force field, a time step of 1 fs, a simulation time of 2000 ps and the canonical ensemble NVT at 303 K. The following equations were used to calculate the adsorption and binding energy [8,13]:

$$E_{adsorption} = E_{interaction} = E_{total} - (E_{surface+solution} + E_{inhibitor}) \quad (8)$$

$$E_{Binding} = -E_{adsorption} = -E_{interaction} \quad (9)$$

where, E_{total} is energy of the whole arrangement, $E_{surface + solution}$ is the total energy of (110) surface of iron and $E_{inhibitor}$ shows the energy of inhibitor.

RESULTS AND DISCUSSION

Weight loss measurements: To investigate the rate of weight of loss (corrosion rate) and rate of mild steel protection (inhibition efficiency), the gravimetric method was applied. For this, mild steel samples were immersed in 1 M HCl with various concentrations of 2POM5PTO at 298-318 K for a period of 12 h [14]. Fig. 1 shows the relation of corrosion rate and inhibition efficiency with the concentration of 2POM5PTO at 298-318 K after 12 h of immersion. It is observed that corrosion rate is inversely proportional with concentration but directly proportional to inhibition efficiency. Fig. 1 defines the inhibition efficiency of the corrosion rate on the optimum concentration at different temperatures is 90.22%, 83.87%, 74.73%, 1.81 mmpy, 3.53 mmpy, 6.81 mmpy, respectively, (Table-1), which implies that more 2POM5PTO molecules were available for the adsorption.

Effect of temperature on corrosion rate and inhibition efficiency: Increased temperature affects the corrosion rate directly and inhibition efficiency inversely, which means that corrosion rate increases while efficiency decreases [15]. This behaviour of inhibitor is due to the number of molecules present in the solution. When the concentration of 2POM5PTO increased, the number of molecules also increases, which got adsorbed on the mild steel's active site and blocked them for further reaction at the metal/solution interface, increasing the temperature, the corrosion rate of reaction increases. Also, the higher temperature reduces the strength of the adsorption action and desorption of the studied corrosion inhibitors from the mild steel surface [16]. The results (Table-1) define that the rate of weight loss decreases and the percentage protection efficiency (η_w%) increases with inhibitor concentration [17].

Adsorption and thermodynamics study: Weight loss measurements suggest that 2POM5PTO forms a thin layer on mild steel surface, which behaves as a barrier. The formed thin layer protects the mild steel surface from corrosion attack of acidic environment. The protective layer formed *via* the replacement of previously adsorbed molecules by 2POM5PTO through the quasi-substitution process. The replacement of water molecules by 2POM5PTO atoms can be represented as follows [18]:

$$Inh_{(sol)} + xH_2O_{(ads)} = Inh_{(ads)} + yH_2O_{(sol)} \quad (10)$$

where $Inh_{(sol)}$ inhibitor dissolved in aggressive media, $H_2O_{(ads)}$ molecules of water, y represent some H_2O replaced by inhibitor molecules, $Inh_{(ads)}$ inhibitor molecules adsorbed on the electrode surface and $H_2O_{(sol)}$ represent H_2O of solution. This way, semi-replacement measure works with the adsorption of 2POM5PTO

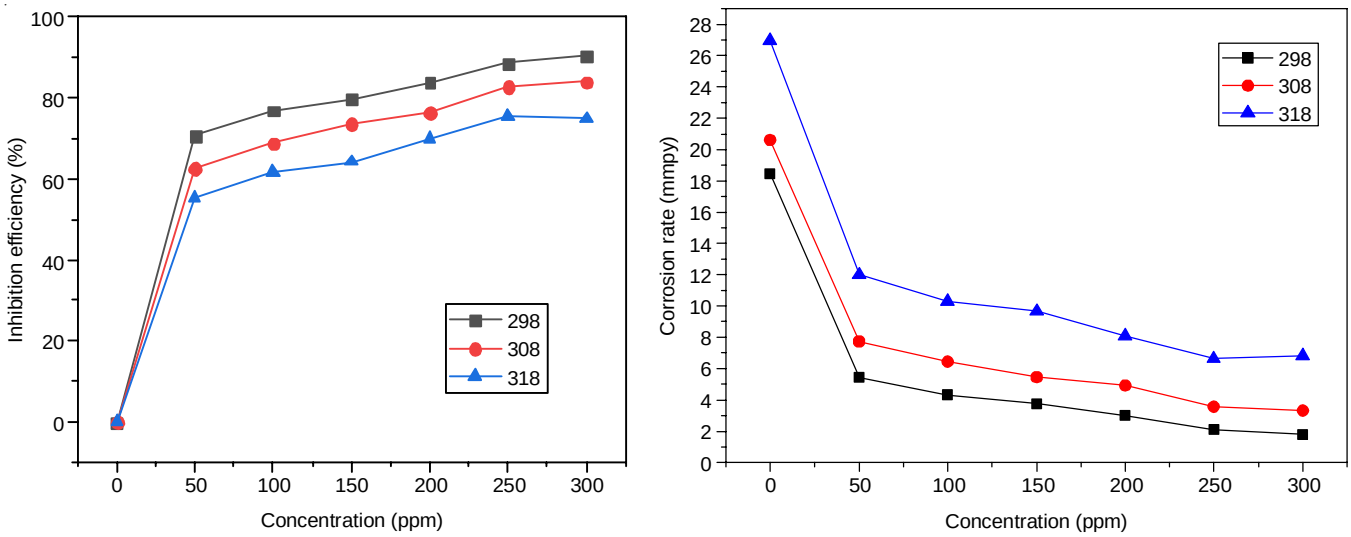

Fig. 1. Plot of $\eta_{w\%}$ and CR with a concentration of 2POM5PTO in 1 M HCl for mild steel

TABLE-1
WEIGHT LOSS CALCULATIONS FOR MS IN 1 M HCl WITHOUT AND WITHIN OF 2POM5PTO AT DIFFERENT TEMPERATURE

Immersion period (h)	Conc. (ppm)	298 K			308 K			318 K		
		CR (mm y^{-1})	η_w (%)	θ	CR (mm y^{-1})	η_w (%)	θ	CR (mm y^{-1})	η_w (%)	θ
12 h	0	18.4718	–	–	20.6263	–	–	26.96	–	–
	50	5.41797	70.66	0.71	7.7309	62.51	0.62	12.00	55.46	0.55
	100	4.30903	76.67	0.77	6.43186	68.17	0.69	10.29	61.81	0.62
	150	3.7704	79.58	0.79	5.44965	73.57	0.74	09.66	64.16	0.64
	200	3.00998	83.70	0.83	4.91102	76.19	0.76	08.08	70.03	0.70
	250	2.12283	88.50	0.88	3.5803	82.64	0.83	06.63	75.44	0.75
	300	1.81	90.22	0.90	3.33	83.87	0.84	06.81	74.73	0.74

atoms on mild steel surfaces. The adsorption of the 2POM5PTO atom is concerned with its surface acquiring ability. The viability of the consumption of inhibitors is the function of surface coverage. The surface coverage (θ) is associated with the doses (C) of an inhibitor [19]. It has been observed that the weight loss measurement data fitted well with the Langmuir isotherm. It confirms that the adsorption behaviour of 2POM5PTO obeys the Langmuir adsorption isotherm interpreted by the following:

$$\frac{C_{inh}}{\theta} = \frac{1}{K_{ads}} + C \quad (11)$$

where, K_{ads} adsorption constant.

Fig. 2 displays a regression coefficient (R^2) of 0.99 with a straight line. It signifies that the 2POM5PTO molecule adsorbs near each other without any satiric hindrance.

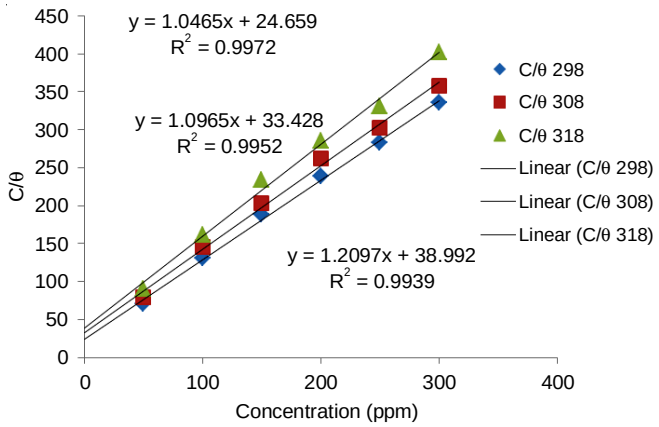

Fig. 2. Plots of Langmuir adsorption isotherms of 2POM5PTO for mild steel at different temperatures

The standard Gibbs (G°_{ads}) free energy of adsorption is crucial for analyzing adsorption continuity. It can be calculated by using K_{ads} as follows:

$$\Delta G^\circ_{ads} = -RT \ln (1 \times 10^6 K_{ads}) \quad (12)$$

where, 10^6 is the water concentration in solution (mol/L), R (8.314 J mol^{-1} K^{-1}) gas constant and T (K) is the absolute temperature. The values of K_{ads} and ΔG°_{ads} were calculated from the graph and the values are presented in Table-2, which indicates that K_{ads} decreases with increasing the temperature. The higher value of K_{ads} at low temperature shows that the adsorption of corrosion inhibitor on mild steel surfaces is substitutional [8].

TABLE-2
ADSORPTION PARAMETERS OF 2POM5PTO IN 1 M HCl SOLUTION AT DIFFERENT TEMPERATURES

Temp. (K)	R^2	K_{ads} (g L^{-1})	Slope	ΔG° (kJ/mol)
298	0.997	24.66	1.046	-27.05
308	0.995	33.43	1.096	-27.18
318	0.993	38.99	1.209	-27.65

Corrosion inhibitor adsorbs spontaneously on mild steel surface, which gave a negative value of ΔG°_{ads} at different temperatures. Corrosion inhibitor has strong interaction with metal depend on the high-value ΔG°_{ads}. It is mainly observed that when ΔG°_{ads} -20 kJ/mol or below, it indicates that the solid electrostatic interaction and defines that molecules of inhibitor show physical adsorption [20]. When -40 kJ/mol or more negative describes the enrolment of coordinate bond formed between inhibitor molecule and mild steel *d*-orbital's is called chemical adsorption (chemisorptions) [21]. In the present investigation, obtained ΔG°_{ads} vary from -27.05 to -27.65, as shown in Table-2 for 2POM5PTO, which indicates that inhibitor molecule adsorbs through both processes physical and chemical on the mild steel surface.

Thermodynamic parameters: The apparent activation energy (E_a) of deterioration of mild steel sample in 1 M HCl containing various concentrations of 2POM5PTO was determined using Arrhenius plot (Fig. 3) according to eqn. 13 [22,23]:

$$\ln CR = A - \frac{E_a}{RT} \quad (13)$$

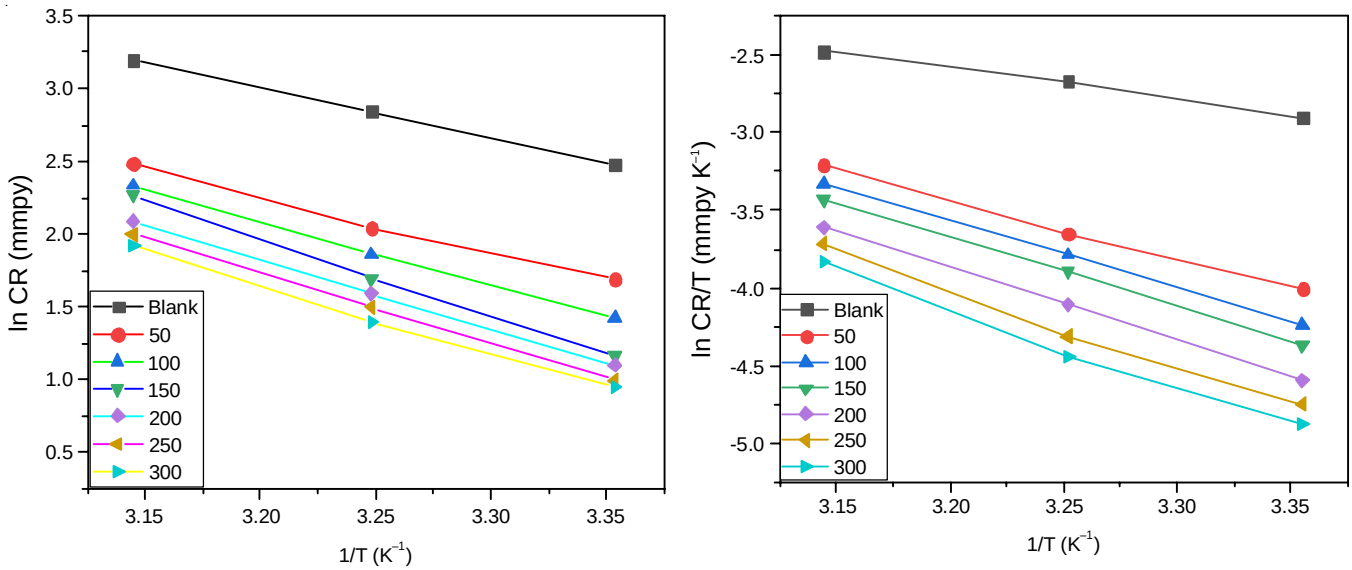

Fig. 3. Plot of ln CR *vs.* 1/T and ln CR/T *vs.* 1/T with and without 2POM5PTO in 1 M HCl for mild steel

where A, Arrhenius pre-exponential factor, T, gas constant and R, temperature, respectively.

Table-3 represents the calculated E_a value for mild steel dissolution in 1 M HCl with an optimum concentration is 57.32 kJ mol^{-1} and in bare1 M HCl is 23.14 kJ mol^{-1}. The comparison of both values defined that activation energy for the corrosion process increased. Therefore, corrosion inhibition takes place *via* a physical adsorption mechanism [24,25].

TABLE-3
COMPUTED THERMO-PARAMETERS FOR MILD STEEL IN 1 M HCl CONTAINING 2POM5PTO AND IN 1 M HCl

Conc. (ppm)	E_a (kJ mol^{-1})	$\Delta H^{\#}$ (kJ mol^{-1})	$\Delta S^{\#}$ (J $mol^{-1}K^{-1}$)
Blank	23.14	16.60	-154.04
50	31.31	31.34	-125.81
100	39.59	39.31	-117.73
150	41.47	37.05	-109.70
200	38.88	38.40	-105.22
250	48.92	44.80	-088.44
300	57.32	45.95	-085.24

Plot between CR/T *vs*. 1/T gave the enthalpy change and entropy change, which can be calculated by using the equation of transition state theory [25]:

$$CR = \frac{RT}{Nh}\exp\left(\frac{\Delta S^{\#}}{R}\right)\exp\left(\frac{-\Delta H^{\#}}{RT}\right) \quad (14)$$

where h, Planck's constant (6.626×10^{-34} J s) and N, Avogadro's number (6.022×10^{23} mol^{-1}).

From the analysis of Table-3, one can say that the mild steel dissolution process is endothermic and the value of $\Delta H^{\#}$ is positive. The highest value of $\Delta H^{\#}$ 45.95 kJ mol^{-1} at 300 ppm concentration (2POM5PTO) and 16.60 kJ mol^{-1} for a blank solution (0 ppm) implies a slow dissolution rate of mild steel. Additionally, significant and negative values of $\Delta S^{\#}$ indicate that the activated complex in the rate-determining step presents an association rather than a dissociation step [26-28].

The comparison between the entropy of uninhibited solution and inhibited in 1 M HCl media shows that blank (1 M HCl) solution has a more negative (–15.04 J mol^{-1} K^{-1}) $\Delta S^{\#}$ value than inhibited (–85.24 J mol^{-1} K^{-1}). This satisfies H_2O desorption from mild steel surface in the presence of 2POM5PTO lead to increase solvent (H_2O) entropy [29,30].

Polarization studies: Polarization experiments have been performed potentiodynamically to understand the anodic and cathodic reaction in 1 M HCl containing various concentrations of 2POM5PTO and in blank. Fig. 4 represents the polarization

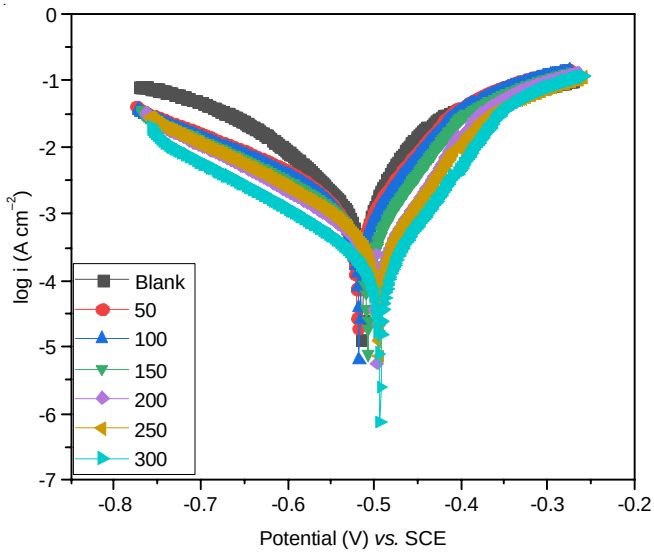

Fig. 4. Tafel polt of mild steel in 1 M HCl solution without and with the presence of various concentrations of 2POM5PTO

curves. The data calculated by extrapolating of tafel plot are shown in Table-4. In acidic solutions, on anode working electrode start dissolving and on cathode evolution of hydrogen and charge-discharge take place inhibitors may affect both reactions anodic (β_a) as well as cathodic (β_c) or one of them either anodic or cathodic [31,32]. The percentage inhibition efficiency ($\eta_{PDP\%}$) can be defined by the following eqn. 15 using the corrosion current densities without (I^{i}_{corr}) and with (I^{o}_{corr}) different concentrations of the inhibitor [33].

$$\eta_{pol}\ (\%) = \left(1 - \frac{I^{i}_{corr}}{I^{o}_{corr}}\right) \times 100 \quad (15)$$

Table-4 shows no change in E_{corr} when inhibitor added and electron current density (I_{corr}) decline with increasing concentration of 2POM5PTO. Furthermore, Tafel curves do not change, indicating that inhibitors could block the anodic and cathodic reactions [34].

When E_{corr} values are > 85 mV, an inhibitor is classed as either anodic or cathodic, but in the present investigation, E_{corr} is < 85, which implies that 2POM5PTO is a mixed type inhibitor. At each concentration of 2POM5PTO, a greater value of anodic constant (β_a) than cathodic constant (β_c) also defines that the inhibitor is a mixed type. The obtained inhibition efficiencies values are in good agreement with those obtained by gravimetric measurements.

EIS studies: Fig. 5a represents a Nyquist plot obtained for mild steel corrosion in 1 M HCl containing different concen-

TABLE-4
POTENTIODYNAMIC POLARIZATION PARAMETERS FOR VARIOUS CONCENTRATIONS OF 2POM5PTO

Conc. (ppm)	β_a (mV dec^{-1})	β_c (mV dec^{-1})	$-E_{corr}$ (mV *vs.* SCE)	I_{corr} (mA cm^{-2})	η_{pol} (%)
Blank	116.53	128.40	312.90	1.917	–
50	119.78	105.76	333.06	0.692	63.90
100	172.44	108.33	356.81	0.611	68.12
150	161.08	95.56	387.11	0.506	73.60
200	105.11	147.13	341.53	0.423	77.93
250	114.66	102.49	363.52	0.392	79.55
300	087.80	102.19	343.93	0.279	85.44

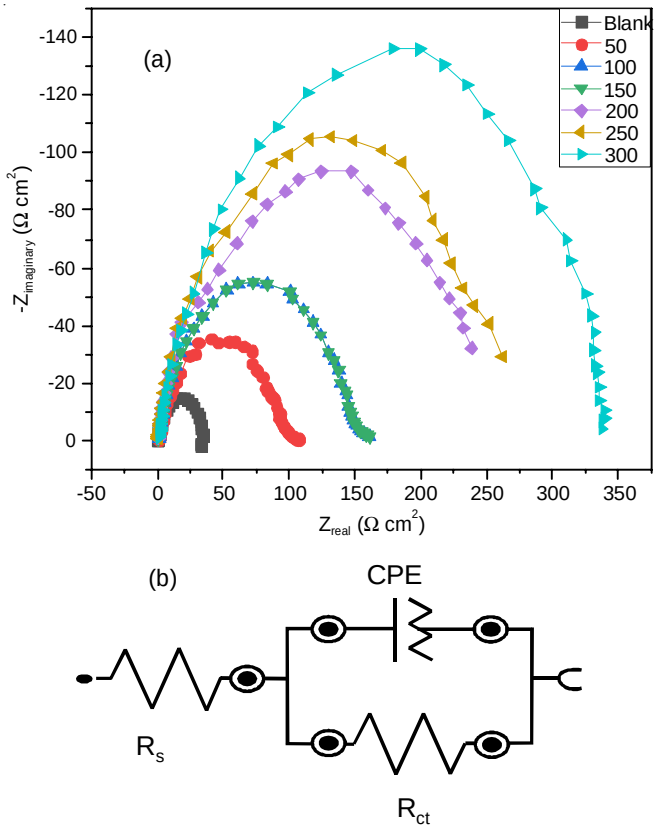

Fig. 5. Nyquist plots for mild steel in 1 M HCl solution containing various concentrations of 2POM5PTO at 298 K

trations of 2POM5PTO at 298 K. The Nyquist plot is made up of capacitive-like semi-circles but with a defect. The plot indicates that 2POM5PTO protects mild steel from corrosion *via* the adsorption process, in which molecules of inhibitor adsorb on the metal surface. The disturbance is seen in a semi-circle because of frequency scattering and the electrode surface. The double-layer capacitance also affects the semi-circle [35,36].

The diameter of the semi-circle rises on increasing inhibitor concentration, which represents that charge transfer helps in corrosion control. The equivalent circuit displayed (where R_s denotes the solution resistance, R_{ct} is the charge-transfer resistance and CPE is a constant phase element) in Fig. 5b was fitted using Zview software to calculate other parameters. First, double-layer capacitance was calculated by using eqn. 17 [37]. Next, the CPE impedance is expressed in eqn. 16 [38]:

$$Z_{CPE} = \left(\frac{1}{Y^o}\right)[(j\omega)_n]^{-1} \quad (16)$$

$$C_{dl} = (Y^o R_{ct}^{1-n})^{1/n} \quad (17)$$

where, Y^o denotes admittance and R_{ct} represents charge transfer resistance along with various concentrations of inhibitors molecule, respectively. The percentage inhibition efficiency was measured by adopting a value of R_{ct} according to the following relation:

$$\eta_{eis}\ (\%) = \frac{R_{ct(inh)} - R_{ct}}{R_{ct(inh)}} \times 100 \quad (18)$$

R_{ct} and $R_{ct\ (inh)}$ represent the charge transfer resistance in the absence and presence of different concentrations of inhibitor molecules, respectively. The EIS data was obtained from equivalent circuit fit tabulated in Table-5. R_{ct} data show increment with concentration, whereas C_{dl} decrease. This defends the capability of (2POM5PTO) thin layer formation and acutely protection of mild steel from corrosion in aggressive media [39,40].

The decrement in double-layer thickness and dielectric constant is supported by decreased value of double-layer capacitance [41]. Consequently, the inhibition efficiency increased with increment in the concentration of 2POM5PTO, reaching 89.86% at 300 ppm.

Surface study

SEM analysis: The surface characterization of mild steel polished surface with and without several concentrations of 2POM5PTO in 1 M HCl immersed for 12 h at 298 K is depicted in Fig. 6a-b. Fig. 6a displays the surface of mild steel, which is highly corroded, broken, damaged and rough due to corrosion. However, at 300 ppm concentration of inhibitor, the morphology of mild steel surface is less corroded and becomes smoother as shown in Fig. 6b. Consequently, the results recommended forming an inhibitive layer on mild steel surface with the addition of 300 ppm concentrations of corrosion inhibitor in 1 M HCl, which may inhibit the surface of mild steel from a corrosive media. Furthermore, the surface of mild steel specimen was substantially protected by the inhibitor, which implies the development of the inhibitive coating of inhibitors.

Energy dispersive X-ray analysis: EDAX spectroscopy may be accomplished to conclude the elemental composition of mild steel specimens in 1 M HCl in the presence of 300 ppm concentration of 2POM5PTO for 12 h immersion at 298 K.

Moreover, the atomic percentage of elements acquired from EDAX spectroscopy investigation is 78.18% O, 8.65% Fe and 1.76% Cl, for an uninhibited solution. Besides, the

TABLE-5
ELECTROCHEMICAL IMPEDANCE PARAMETERS OF MILD STEEL WITHOUT AND WITHIN 2POM5PTO IN 1 M HCl 298 K

Conc. (ppm)	R_{ct} (Ω cm^2)	CPE/$Y_o \times 10^6$ (S cm^{-2} S^{n2})	n	C_{dl} (μF cm^{-2})	η_{eis} (%)
Blank	034.07	219.40	0.8151	1659.35	–
50	106.99	189.11	0.8292	1451.75	68.15
100	130.64	163.90	0.8241	1377.01	73.92
150	159.81	154.40	0.8252	1315.37	78.68
200	237.67	139.11	0.8152	1260.89	85.66
250	239.59	128.41	0.8301	1064.60	85.77
300	336.31	109.41	0.8292	0953.95	89.86

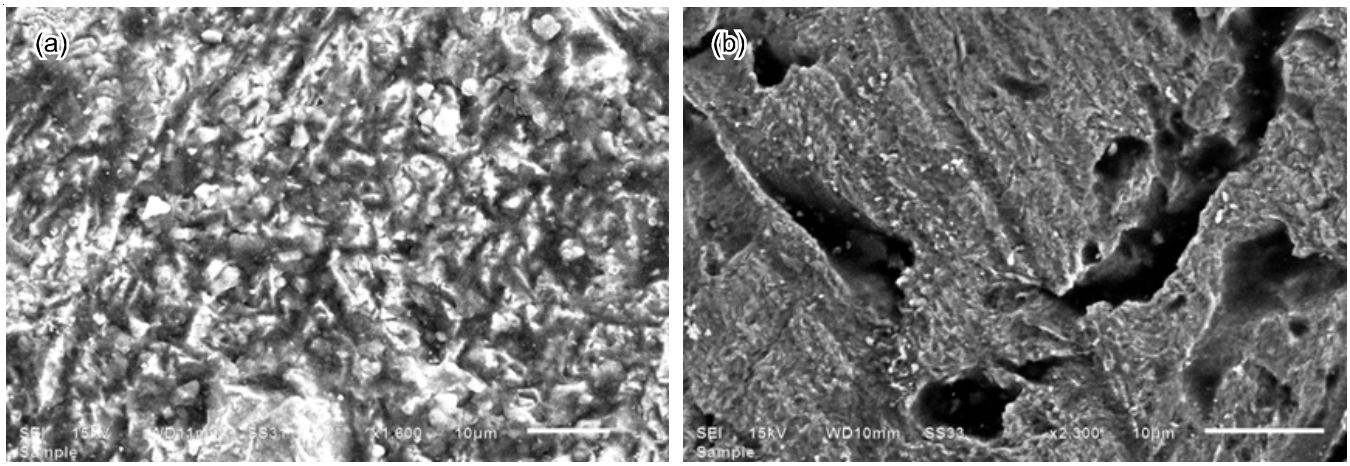

Fig. 6. SEM images for mild steel (a) 1 M HCl solution (b) 2POM5PTO at 298 K

percentage elements composition for 300 ppm concentration is 56.91% O, 6.58% N, 6.65% Fe, 27.77% C and 1.71% Cl, for inhibited solution. The peak of oxygen in case of inhibitor significantly decreased, which concludes that there is a decrease in a density of corrosion active centers and confirms the existence of used inhibitors concentration in 1 M HCl (Fig. 7). Further, all these experimental data explains that inhibitor forms a protective layer through strong adsorption on mild steel surface to protect against corrosion. Additionally, all these experimental data demonstrate that inhibitor begins a protective layer through strong adsorption on mild steel surface to protect against corrosion.

Quantum chemical calculations (DFT): The DFT analysis provides a significant knowledge of the corrosion inhibition mechanism. The experimental results correlated with DFT parameters such as E_{HOMO}, E_{LUMO}, ν, ΔN and χ were carried out to study the effectiveness of 2POM5PTO on the protective mechanism of mild steel from corrosion in 1 M HCl solution. The optimized structure, highest occupied molecular orbital (HOMO), lowest occupied molecular orbital (LUMO) diagrams of 2POM5PTO are shown in Fig. 8. According to the E_{HOMO} value, one can say that the inhibitors donate electrons easily to empty *d*-orbital of metal; on the other hand, E_{LUMO} says that inhibitors can accept electrons from the metal (Table-6). Therefore, the donation and acceptance capability of the inhibitor protects the metal from corrosion attack also supports the adsorptive mechanism. The ΔN value indicates that transfer of electron takes place inhibitor to metal.

Mulliken charge distribution: Mulliken charge analysis performs for the local reactivity, donor-acceptor electron inter-

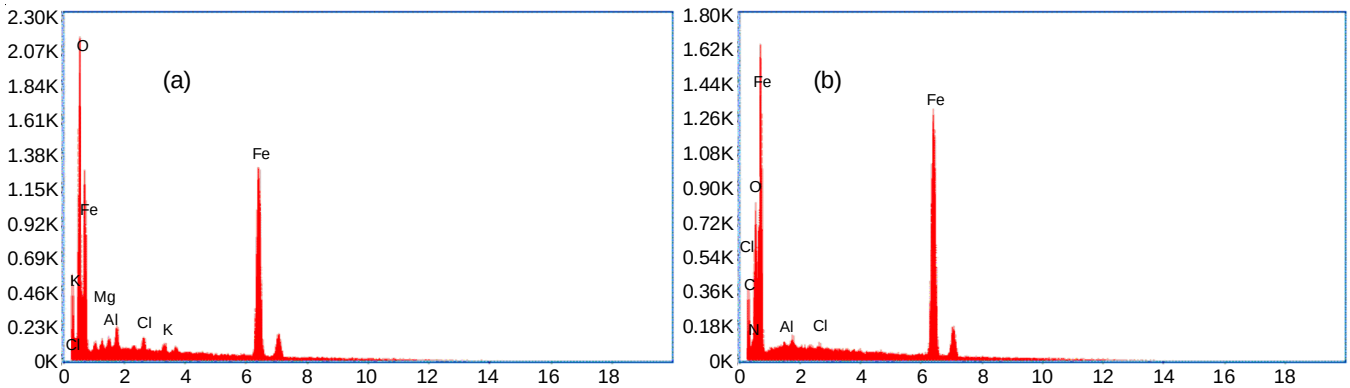

Fig. 7. EDAX spectrum for mild steel surface (a) 1 M HCl solution (b) with 300 ppm concentration of 2POM5PTO at 298 K for an immersion period of 12 h

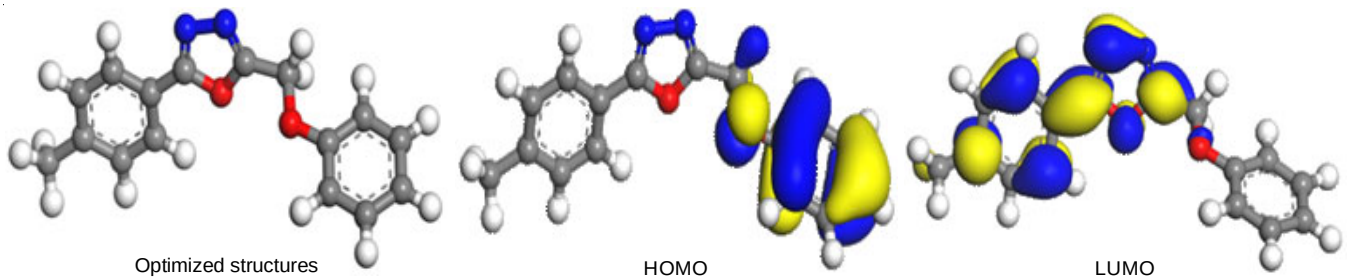

Fig. 8. DFT-derived geometry optimized structure, HOMO and LUMO of 2POM5PTO

TABLE-6
VARIOUS QUANTUM CHEMICAL VARIABLES FOR 2POM5PTO EMPLOYING HYBRID FUNCTIONAL

E_{HOMO} (eV)	E_{LUMO} (eV)	ΔE (eV)	μ (D)	χ (eV)	ΔN (eV)
-5.699	-2.573	3.126	5.174	4.136	0.535

TABLE-7
LOCAL REACTIVE SITES FOR 2POM5PTO

Atoms	f_k^+	f_k^-	Δf (k) ($f_k^+ - f_k^-$)	Atoms	f_k^+	f_k^-	Δf (k) ($f_k^+ - f_k^-$)
H (1)	0.3	6.4	-6.1	C (18)	11.1	0.7	10.4
C (2)	0.3	8.9	-8.6	C (19)	2.8	-0.1	2.9
C (3)	0.2	5.4	-5.2	C (20)	6.8	0.2	6.6
C (4)	-0.1	7.2	-7.3	C (21)	6.5	0.2	6.3
C (5)	0.2	4.1	-3.9	C (22)	7.0	0.2	6.8
C (6)	0.3	11.8	-11.5	C (23)	2.7	0.1	2.6
C (7)	0.2	8.0	-7.8	C (24)	2.9	0.1	2.8
H (8)	0.3	5.3	-5.0	H (25)	4.5	0.2	4.3
H (9)	0.3	6.9	-6.6	H (26)	4.3	0.1	4.2
H (10)	0.3	5.6	-5.3	H (27)	3.7	0.1	3.6
H (11)	0.3	5.6	-5.3	H (28)	3.7	0.2	3.5
O (12)	-0.1	13.1	-13.2	C (29)	-0.5	0	-0.5
C (13)	1.1	-3.0	4.1	H (30)	3.2	0.1	3.1
H (14)	2.1	4.9	-2.8	H (31)	2.3	0.1	2.2
H (15)	2.8	5.0	-2.2	H (32)	2.3	0.1	2.2
C (16)	7.8	0	7.8	N (33)	5.4	1.4	4.0
O (17)	5.4	0.3	5.1	N (34)	9.5	0.7	8.8

action between inhibitor molecules and iron. Generally, the atom with a negative charge behaves as a nucleophile and gets adsorbed on metal surfaces through electron donation [13]. On the other hand, atoms with a positive charge get adsorbed on a metal surface by accepting electrons. Therefore, the analysis of the optimized molecular structure represented in Fig. 9 and Mulliken charges (Table-7) of the inhibitor (2POM5PTO) implies that molecules inhibitor can be effectively adsorbed on the steel surface to inhibit metal corrosion.

Molecular dynamic (MD) simulations: The MD was conducted to understand the interaction between these inhibitor molecules (adsorbate) and iron (110). The system's binding energy and total energy were obtained on equilibrium position by using eqns. 8 and 9 [42]. Fig. 10 represents the simulation module's side and top views of the final most stable adsorption configurations for 2POM5PTO-Fe (110) systems.

Analysis of Fig. 10 concluded that Fe-atom protected by the inhibitor through adsorption. The current adsorption model explains strong interactions by extension, high alluding to the experimental result [42]. Table-8 shows interaction energy and

TABLE-8
VARIOUS ENERGY VARIABLES MEASURED
FROM MD SIMULATIONS FOR 2POM5PTO

E_{total} (kcal/mol)	$E_{surface + solution}$ (kcal/mol)	$E_{binding}$ (kcal/mol)
-17091.307	17151.984	29.879

binding energy calculated from the MD study, implying that 2POM5PTO adsorbed inhibitor onto the Fe-surface in HCl solution.

Conclusion

A new molecule, 2-(phenylmethyl)-5-*p*-tolyl-1,3,4-oxadiazole (2POM5PTO) was examined as a new corrosion inhibitor on mild steel surface in 1 M HCl. From the varying experiment's conditions, it could be decided that the used corrosion inhibitor performs as an efficient inhibitor in 1 M HCl. The weight loss estimation shows that enhancing the inhibitor concentration in acidic solution enhances the inhibition efficiency, but the corrosion rate diminishes. Potentiodynamic polarization plots signified that the inhibitor was mixed type by combining the hydrogen evolution and metal disintegration reaction.

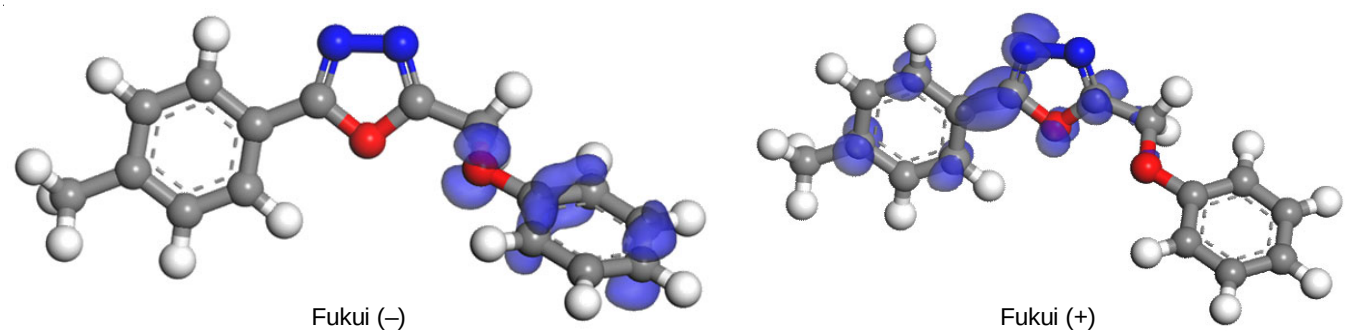

Fig. 9. Fukui indices position expressed for 2POM5PTO molecules

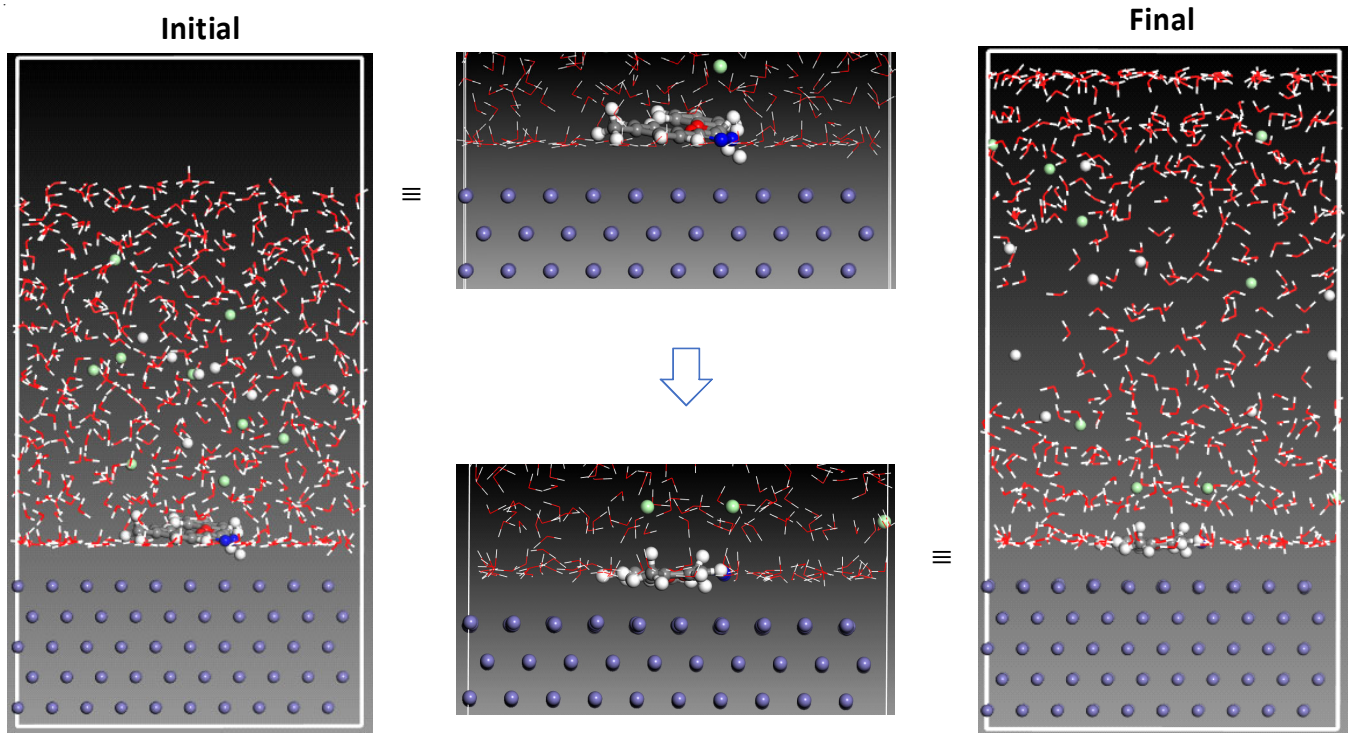

Fig. 10. Initial and final sight of studied inhibitors adsorption 2POM5PTO

Electrochemical impedance examination exhibits that charge transfer resistance enhances value, but double-layer capacitance diminishes with improving the inhibitor concentration. The adsorption phenomenon obeys the Langmuir adsorption isotherm. The value enthalpy of activation was positive, which explains that the destruction of mild steel is endothermic. The entropy of activation indicates the decline in the rate of metal dissolution. The thermodynamic parameters of the adsorption process imply the adsorption behaviour was spontaneous and physical. The SEM and EDAX analysis of mild steel surface exposed the evolution of the inhibitive film of 2POM5PTO inhibitors on the surface of mild steel. All the results acquired from different techniques were in the reasonable agreement. The quantum parameters E_{HOMO}, E_{LUMO}, dipole movement, ΔN favours the good inhibition efficiency and correlation with experimental results. The binding and interaction energy of molecular dynamic simulation support the chemi-sorptions and agreed with the practical efficiency.

ACKNOWLEDGEMENTS

The authors are grateful to the Department of Chemistry, Maharshi Dayanand University, Rohtak, India, to be facilitated with well-equipped technical assistance. Furthermore, one of the authors, Suresh Kumar is highly grateful to the Council of Scientific and Industrial research (CSIR-HRDG), New Delhi, India, for availing Fellowship number. 09/382(0186)/2017-EMR-I.

CONFLICT OF INTEREST

The authors declare that there is no conflict of interests regarding the publication of this article.

REFERENCES

1. J. Aslam, R. Aslam, S.H. Alrefaee, M. Mobin, A. Aslam, M. Parveen and C. Mustansar Hussain, *Arab. J. Chem.*, **13**, 7744 (2020); https://doi.org/10.1016/j.arabjc.2020.09.008
2. F. Boudjellal, H.B. Ouici, A. Guendouzi, O. Benali and A. Sehmi, *J. Mol. Struct.*, **1199**, 127051 (2020); https://doi.org/10.1016/j.molstruc.2019.127051
3. M. Finšgar and J. Jackson, *Corros. Sci.*, **86**, 17 (2014); https://doi.org/10.1016/j.corsci.2014.04.044
4. M. Goyal, S. Kumar, I. Bahadur, C. Verma and E.E. Ebenso, *J. Mol. Liq.*, **256**, 565 (2018); https://doi.org/10.1016/j.molliq.2018.02.045
5. Y. Ye, Y. Zou, Z. Jiang, Q. Yang, L. Chen, S. Guo and H. Chen, *J. Alloys Compd.*, **815**, 152338 (2020); https://doi.org/10.1016/j.jallcom.2019.152338
6. Y. Ye, D. Yang, H. Chen, S. Guo, Q. Yang, L. Chen, H.C. Zhao and L. Wang, *J. Hazard. Mater.*, **381**, 121019 (2020); https://doi.org/10.1016/j.jhazmat.2019.121019
7. Y. Ye, Z. Jiang, Y. Zou, H. Chen, S. Guo, Q. Yang and L. Chen, *J. Mater. Sci. Technol.*, **43**, 144 (2020); https://doi.org/10.1016/j.jmst.2020.01.025
8. V. Kalia, P. Kumar, S. Kumar, P. Pahuja, G. Jha, S. Lata and H. Dahiya, *J. Mol. Liq.*, **313**, 11360 (2020); https://doi.org/10.1016/j.molliq.2020.113601
9. P. Niu, J. Kang, X. Tian, L. Song, H. Liu, J. Wu, W. Yu and J. Chang, *J. Org. Chem.*, **80**, 1018 (2015); https://doi.org/10.1021/jo502518c
10. S.K. Saha, *Phys. Chem. Chem. Phys.*, **8**, 17898 (2016); https://doi.org/10.1039/C6CP01993E
11. M. Edrakia, I.M. Moghadam, M.B. Keivanic and M.H. Fekri, *Iran. Chem. Commun.*, **7**, 228 (2019); https://doi.org/10.30473/icc.2018.42617.1486
12. H. Lgaz, I.-M. Chung, R. Salghi, I.H. Ali, A. Chaouiki, Y. El Aoufir and M.I. Khan, *Appl. Surf. Sci.*, **463**, 647 (2019); https://doi.org/10.1016/j.apsusc.2018.09.001
13. W. Zhang, H.-J. Li, L. Chen, S. Zhang, Y. Ma, C. Ye, Y. Zhou, B. Pang and Y.-C. Wu, *Carbohydr. Polym.*, **238**, 116216 (2020); https://doi.org/10.1016/j.carbpol.2020.116216

14. H. Khaleel, A.A. Ateeq and A.A. Ali, *Int. J. Appl. Eng. Res.*, **13**, 3638 (2018).
15. A. Anees, *J. Chil. Chem. Soc.*, **3**, 2545 (2014).
16. F. El-Taib Heakal, M.A. Deyab, M.M. Osman and A.E. Elkholy, *Desalination*, **425**, 111 (2018); https://doi.org/10.1016/j.desal.2017.10.019
17. I.B. Onyeachu, M.M. Solomon, S.A. Umoren, I.B. Obot and A.A. Sorour, *Desalination*, **479**, 114283 (2020); https://doi.org/10.1016/j.desal.2019.114283
18. D.B. Tripathy, M. Murmu, P. Banerjee and M.A. Quraishi, *Desalination*, **472**, 114128 (2019); https://doi.org/10.1016/j.desal.2019.114128
19. Y. Zhou, S. Xu, L. Guo, S. Zhang, H. Lu, Y. Gong and F. Gao, *RSC Adv.*, **5**, 14804 (2015); https://doi.org/10.1039/C4RA14449J
20. A. Dutta, S.K. Saha, U. Adhikari, P. Banerjee and D. Sukul, *Corros. Sci.*, **123**, 256 (2017); https://doi.org/10.1016/j.corsci.2017.04.017
21. M. Murmu, S.K. Saha, N.C. Murmu and P. Banerjee, *Corros. Sci.*, **146**, 134 (2019); https://doi.org/10.1016/j.corsci.2018.10.002
22. M. Faustin, A. Maciuk, P. Salvin, C. Roos and M. Lebrini, *Corros. Sci.*, **92**, 287 (2015); https://doi.org/10.1016/j.corsci.2014.12.005
23. M.A. Deyab and S.S.A. El-Rehim, *J. Taiwan Inst. Chem. Eng.*, **45**, 1065 (2014); https://doi.org/10.1016/j.jtice.2013.09.004
24. M. Bahrami, S. Hosseini and P. Pilvar, *Corros. Sci.*, **52**, 2793 (2010); https://doi.org/10.1016/j.corsci.2010.04.024
25. M. Hegazy, M. Abdallah and H. Ahmed, *Corros. Sci.*, **52**, 2897 (2010); https://doi.org/10.1016/j.corsci.2010.04.034
26. A.H. Alamri, *Desalination*, **470**, 114100 (2019); https://doi.org/10.1016/j.desal.2019.114100
27. F. El-Taib Heakal, A.S. Fouda and M.S. Radwan, *Mater. Chem. Phys.*, **125**, 26 (2011); https://doi.org/10.1016/j.matchemphys.2010.08.067
28. T. Poornima, J. Nayak and A. Nityananda Shetty, *Corros. Sci.*, **53**, 3688 (2011); https://doi.org/10.1016/j.corsci.2011.07.014
29. S. Banerjee, V. Srivastava and M. Singh, *Corros. Sci.*, **59**, 35 (2012); https://doi.org/10.1016/j.corsci.2012.02.009
30. D.K. Yadav, M. Quraishi and B. Maiti, *Corros. Sci.*, **55**, 254 (2012); https://doi.org/10.1016/j.corsci.2011.10.030
31. A.Y. Musa, A.A.H. Kadhum, A.B. Mohamad, A.A.B. Rahoma and H. Mesmari, *J. Mol. Struct.*, **969**, 233 (2010); https://doi.org/10.1016/j.molstruc.2010.02.051
32. M. Ouakki, M. Galai, M. Rbaa, A.S. Abousalem, B. Lakhrissi, E.H. Rifi and M. Cherkaoui, *Heliyon*, **5**, e02759 (2019); https://doi.org/10.1016/j.heliyon.2019.e02759
33. J.A. Syed, S. Tang, H. Lu and X. Meng, *Ind. Eng. Chem. Res.*, **54**, 2950 (2015); https://doi.org/10.1021/ie5046395
34. C.B. Verma, M.A. Quraishi and E.E. Ebenso, *Int. J. Electrochem. Sci.*, **9**, 5537 (2014).
35. S.A. Umoren, U.M. Eduok, M.M. Solomon and A.P. Udoh, *Arab. J. Chem.*, **9**, S209 (2016); https://doi.org/10.1016/j.arabjc.2011.03.008
36. N.B. Iroha and N.J. Maduelosi, *ISOR J. Appl. Chem.*, **13**, 30 (2020).
37. N.O. Eddy, H. Momoh-Yahaya and E.E. Oguzie, *J. Adv. Res.*, **6**, 203 (2015); https://doi.org/10.1016/j.jare.2014.01.004
38. M. Kraljic Rokovic, K. Kvastek, V. Horvat-Radoševic and L. Duic, *Corros. Sci.*, **49**, 2567 (2007); https://doi.org/10.1016/j.corsci.2006.12.010
39. K.F. Khaled, *Mater. Chem. Phys.*, **112**, 290 (2008); https://doi.org/10.1016/j.matchemphys.2008.05.056
40. A.O. James and N.B. Iroha, *ISOR J. Appl. Chem.*, **12**, 1 (2019).
41. M. Özcan and I. Dehri, *Corros. Sci.*, **54**, 201 (2012); https://doi.org/10.1016/j.corsci.2011.09.013
42. M.E. Belghiti, S. Echihi, A. Dafali, Y. Karzazi, M. Bakasse, H. Elalaoui-Elabdallaoui, L.O. Olasunkanmi, E.E. Ebenso and M. Tabyaoui, *Appl. Surf. Sci.*, **491**, 707 (2019); https://doi.org/10.1016/j.apsusc.2019.04.125